Check for updates

Synthesis of triblock copolymer polydopamine-polyacrylic-polyoxyethylene with excellent performance as a binder for silicon anode lithium-ion batteries

Lei Lü,[ab] Hongming Lou,[a] Yinglin Xiao,[b] Guangzhao Zhang, [ID][c] Chaoyang Wang [ID] *[c] and Yonghong Deng [ID] *[b]

Triblock copolymer polydopamine-polyacrylic-polyoxyethylene (PDA-PAA-PEO) with excellent performance as a binder for silicon anodes was synthesized. Its structure was confirmed by ^{1}H-NMR, FTIR and UV-vis spectroscopy. Results of electrochemical measurements indicated that a silicon anode based on PDA-PAA-PEO binder exhibited excellent cycle performance with a reversible capacity of 1597 mA h g^{-1} after 200 cycles at a current density of 0.5 C, much better than that of an electrode based on a polyvinylidene-fluoride binder. Improvement of the cycle performance and reversible capacity for silicon anodes could be attributed to the strong adhesive and high ion conductivity of PDA-PAA-PEO.

Introduction

Lithium-ion batteries (LIBs) are very promising electrochemical energy-storage devices.[1] As an anode material for LIBs, silicon (Si) has been considered to be an intriguing candidate for next-generation, high-energy-density anode materials for LIBs due to its high theoretical capacity (4200 mA h g^{-1}) and natural abundance.[2,3] However, the drastic volume changes of Si during charging–discharging result in pulverization and rapid capacity fade of Si-based electrodes, which hinders its practical application.[4] Numerous efforts have been proposed to address this problem, including nanostructuring of Si, formation of Si-based alloys and design of alternative binder polymers.[5–9] Extensive research has demonstrated that the binder plays an important part in maintaining electrode integrity, which affects the electrochemical performance of Si-based electrodes directly.[10–12] Polyvinylidene fluoride (PVDF), as a commercial binder for graphite anodes, cannot accommodate the drastic volume expansion of Si anodes effectively due to the weak van der Waals' force between PVDF and active particles. Furthermore, poisonous *N*-methyl pyrrolidines (NMPs), which are expensive, are usually employed as the solvent for PVDF binders, which has limited their application.[13,14] Studies have shown that carboxyl-containing polymers such as carboxymethyl cellulose (CMC) and poly(acrylic acid) (PAA) are excellent binders owing to the formation of hydrogen bonds or covalent bonds between the carboxyl groups of binders and hydroxyl groups on the Si surface, which greatly improves the cycle stability of Si-based electrodes.[15] Extensive research has focused on the modification of carboxyl-containing binders such as PAA-PBI,[16] PAA-PVA,[17] c-PAA-CMC.[18]

Recently, mussels have attracted much attention due to their extraordinary adhesion to almost all types of surfaces, which has been attributed to a catechol functional group.[19–21] Research suggests that catechol-modified polymers with strong adhesion possess could be applied extensively.[21–25] Poly(ethylene oxide) (PEO) is a well-known as solid-state electrolyte in LIBs owing to its high conduction of lithium ions, which is ascribed to the lone-pair electrons on the oxygen of the ether groups.[26,27] PEO-based polymers have been applied as cathode binders to enhance the transport of lithium ions in active materials.[28–30] Besides, the ether moiety can increase the interface adhesion and ductility of binder polymers.[31–34]

Herein, we prepared a triblock copolymer containing the characteristics of ethylene oxide moieties as well as carboxyl and catechol groups, and used it as binder for Si anodes in LIBs. Compared with the Si/PVDF electrode, the Si/PDA-PAA-PEO electrode exhibited more stable cyclic performance and lower electrochemical impedance due to the strong adhesion and high ionic conductivity of PDA-PAA-PEO. Moreover, our results showed that incorporation of catechol groups in the binders could improve the capacities of the electrodes. Furthermore, compared with oil-solvent binding of PVDF, water-solvent PDA-PAA-PEO had much better application prospects because it is environmentally friendly.

[a]School of Chemistry and Chemical Engineering, South China University of Technology, Guangzhou, China, 516640. E-mail: cehmlou@scut.edu.cn

[b]Department of Materials Science and Engineering, Southern University of Science and Technology, Shenzhen, China, 518055. E-mail: yhdeng08@163.com

[c]Research Institute of Materials Science, South China University of Technology Guangzhou, China, 510640

Experimental

Materials

2-Methyl-2-[(dodecylsulfanylthiocarbonyl) sulfanyl] propanoic acid (CTA) and the macro-RAFT agent CTA-PEO-CTA were synthesized following a procedure reported previously.[35,36] Poly(ethylene oxide) (molecular weight = 20 000), trifluoroacetic acid (TFA), EDC·3HCl and dopamine hydrochloride were purchased from Aladdin. Dichloromethane (DCM), diethyl ether, 1,4-dioxane were obtained from Shanghai Lingfeng Chemicals. *tert*-Butyl acrylate (AR; Aladdin) was purified through chromatography by flow through an alkaline aluminum oxide column to remove inhibitors. Azodiisobutyronitrile (99%; Aladdin) was recrystallized twice from methanol. Phosphate-buffered saline (PBS) was obtained by mixing potassium dihydrogen phosphate (KH_2PO_4) with disodium hydrogen phosphate (Na_2HPO_4). Si nanopowder (50 nm, 99.9%), super P and other battery accessories were purchased from Shenzhen Kejing. Electrolytes were obtained from Capchem.

Preparation of the triblock copolymer binder PDA-PAA-PEO

Synthesis of poly(*tert*-butyl acrylate)-*co*-poly(ethylene oxide)-*co*-poly(*tert*-butyl acrylate) (P*t*BA-PEO-P*t*BA). The macro-RAFT agent CTA-PEO-CTA (0.53 g, 0.025 mmol), *t*-butyl acrylate (1.6 mL, 11 mmol) and azodiisobutyronitrile (0.002 g, 0.0125 mmol) were dissolved in 3 mL of dioxane. The mixture was stirred for 12 h in a nitrogen atmosphere at 70 °C. The resulting polymer was precipitated with deionized water and dried under vacuum overnight.

Synthesis of poly(acrylic acid)-*co*-poly(ethylene oxide)-*co*-poly(acrylic acid) (PAA-PEO-PAA). 1.0 g of P*t*BA-PEO-P*t*BA was dissolved in 40 mL of freshly dried and distilled DCM. Then, a tenfold molar excess of TFA with respect to the ester group was added slowly to the solution at 0 °C. The mixture was maintained and stirred at this temperature for 3 h and then for 48 h at room temperature. PAA-PEO-PAA was precipitated in cold diethyl ether and dried under vacuum overnight.

Synthesis of poly(dopamine-acrylic acid)-*co*-polyethylene oxide-*co*-poly(dopamine-acrylic acid) (PDA-PAA-PEO). 0.35 g of PAA-PEO-PAA (3 mmol of AA groups) was dissolved in 30 mL of PBS (0.1 M). This was followed by the addition of 0.9 mmol of EDC·3HCl (173 mg) and 0.9 mmol of dopamine hydrochloride (171 mg) into the solution. The mixture was stirred for 24 h after adjusting the pH to 6.0 with 1.0 M NaOH and HCl. The reaction mixture was dialyzed using a regenerated cellulose dialysis membrane (cutoff molecular weight: 3500 Da) against deionized water until Cl^- was undetectable in the washing solution. A "fluffy" gray solid was obtained after freeze-drying.

Characterization and measurements

Structural characterization. Proton nuclear magnetic resonance (¹H-NMR) was carried out on an Ascend™ 400 MHz nuclear magnetic resonance spectrometer (Bruker) using chloroform-d or DMSO-d as solvents. Fourier transform infrared (FTIR) spectroscopy was undertaken on a PerkinElmer 70 system using KBr pellets. UV-visible characterization was achieved on a Lambda 950 spectrophotometer (PerkinElmer) using a 1 cm quartz cuvette. Dopamine standard solution with a concentration range of 0–10 mg L^{-1} was prepared. A dopamine standard curve was obtained according to the absorbance of that solution at 280 nm. The content of catechol groups in PDA-PAA-PEO was measured by comparing the absorbance of PDA-PAA-PEO solution (40 mg L^{-1}) with the dopamine standard curve. Elemental analysis was conducted on a Vario EL Cube (Elementar). Gel permeation chromatography (GPC) was done on a Waters 2414 system.

Electrochemical characterization. PDA-PAA-PEO solution was prepared by adding PDA-PAA-PEO into Tris buffer solution (pH = 8.5). PAA-PEO-PAA or PVDF were dissolved in deionized water or *N*-methyl-2-pyrrolidone (NMP) for comparison, respectively, both of which were used as binders. The Si electrode was fabricated through a particular procedure. Briefly, Si NP, binder, and super P at a weight ratio of 60 : 20 : 20 were mixed and stirred for 12 h. Then, the slurries were cast onto copper foils. After the cast films had been dried in a vacuum oven for 12 h at 120 °C, they were cut into wafers of diameter 1.2 cm and then dried under vacuum for 12 h at 120 °C. The mass loading of all active materials was ≈0.4 mg cm^{-2}. 2025-type coin cells were assembled in an argon-filled glove box using lithium foil as counter electrode and Celgard 2400 as a separator. The electrolyte consisted of a solution of 1 M of $LiPF_6$ in a mixture of ethylene carbonate, diethyl carbonate and dimethyl carbonate (EC : DEC : DMC, 1 : 1 : 1 by volume). The cycle performance was tested on a LAND battery test system (Wuhan) at 0.01–1 V. Electrochemical impedance spectroscopy (EIS) and cyclic voltammetry (CV) were employed on an electrochemical workstation (Solartron Analytical).

Peeling test. Before a 180° peeling test, the electrode films were cut into laminates of 12 × 20 mm. The laminates were attached to Scotch Tape™. The peeling force was recorded on a universal testing machine by pulling the Scotch Tape at a constant displacement rate of 5 mm min^{-1}. Each sample was tested thrice to guarantee accuracy.

Results and discussion

PDA-PAA-PEO was obtained by a three-step method. First, P*t*BA-PEO-P*t*BA was synthesized through RAFT polymerization using tBA as a monomer and CTA-PEO-CTA as a chain-transfer agent. Second, PAA-PEO-PAA was obtained by the hydrolysis of P*t*BA-PEO-P*t*BA with excess TFA. Third, –COOH groups in PAA-PEO-PAA reacted with primary amines in dopamine through coupling reactions with EDC·3HCl as a catalytic agent, and PDA-PAA-PEO was obtained (Fig. 1).

The structures of P*t*BA-PEO-P*t*BA and PAA-PEO-PAA were confirmed by the ¹H-NMR spectra (Fig. 2a). The ¹H-NMR spectra of CTA-PEO-CTA showed a singlet at ≈3.6 ppm assigned to –CH₂CH₂O– in PEO blocks. The singlet at ≈1.45 ppm corresponding to *tert*-butyl groups confirmed the structure of P*t*BA-PEO-P*t*BA. The singlet at ≈1.45 ppm disappeared when P*t*BA-PEO-P*t*BA was hydrolyzed to PAA-PEO-PAA. The spectra of PAA-PEO-PAA showed a wide peak at ≈12 ppm that was
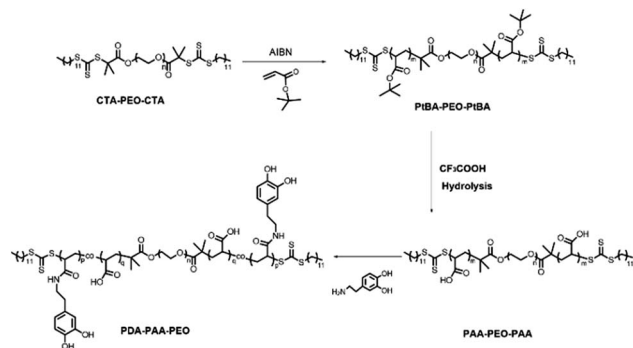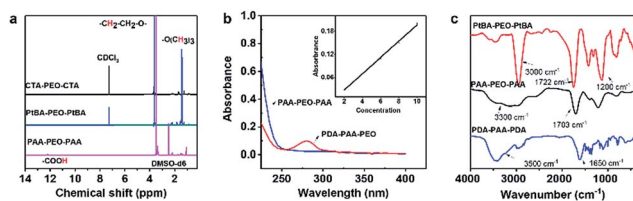
Fig. 1 Synthesis of PDA-PAA-PEO triblock copolymers.

Fig. 2 Structural characteristics of PtBA-PEO-PtBA, PAA-PEO-PAA and PDA-PAA-PEO. (a) ^{1}H-NMR spectra (b) UV spectrum and (c) FTIR spectra.

assigned to –COOH. The structure of PDA-PAA-PEO was verified by a UV spectrum (Fig. 2b). The absorption band at 280 nm was related to the catechol group. According to the standard curve of dopamine (inset in Fig. 2b), the content of dopamine in polymers was ≈13.6%, which corresponded to the results of elemental analysis shown in Table 1. According to GPC, the weight-average molecular weight of PDA-PAA-PEO was 70 795 g mol^{-1}.

All of these structures were verified further by FTIR spectroscopy (Fig. 2c). In the spectra of PtBA-PEO-PtBA, a pointed peak at ≈3000 cm^{-1} was observed, which was assigned to the stretching vibrations of C–H in PtBA blocks. The peaks at 1722 cm^{-1} and 1200 cm^{-1} were attributed to the C=O stretching of ester groups (COOR) and C–O–C stretching of ethylene oxide moieties, respectively. FTIR spectroscopy of PAA-PEO-PAA showed a shift in the position of the C=O stretching band from 1722 cm^{-1} to 1703 cm^{-1} due to the hydrolysis of COOR to COOH, and the pointed peak at ≈3000 cm^{-1} disappeared, which signified the loss of a *tert*-butyl group. A new broad peak at 3300 cm^{-1} was assigned to the stretching vibrations of O–H, which confirmed the existence of –COOH. In the spectra of PDA-PAA-PEO, the peaks at ≈1650 cm^{-1} and

≈3500 cm^{-1} were assigned to the C=O stretching band and N–H stretching band, respectively, which indicated that the amino groups of dopamine had reacted with the carboxyl group, and that amide groups (CONH) were obtained.

These characteristic peaks demonstrated that PDA-PAA-PEO had been synthesized.

We conducted a series of electrochemical measurements to investigate the performance of PDA-PAA-PEO as a binder for Si anodes in LIBs using PAA-PEO-PAA and PVDF binders as reference. CV curves were measured in a potential range between 0.01 V and 2.5 V at a scan rate of 0.05 mV s^{-1} for three cycles (Fig. 3a–c). In the first cycle, a cathodic peak at 1.5 V may have corresponded to formation of a solid electrolyte interphase, which disappeared at the second and third cycles, demonstrating no formation of a new solid electrolyte interphase (SEI) layer on Si surfaces.[37,38] For the CV curve of Si/PDA-PAA-PEO (Fig. 3a), a cathodic peak at 0.1 V was assigned to the formation of Li$_x$Si in the first discharge process; the corresponding charge curve showed peaks at 0.35 V and 0.5 V assigned to the delithiation of Li$_x$Si.[39] The second and third cycles showed the same cathodic and anodic peaks, implying that the lithiation and delithiation reactions were highly reversible.[40,41] A cathodic peak at 2.0 V could be ascribed to the electron transfer between carbonyl groups and lithium ions, a finding that is similar to previous reports.[42] Fig. 3b shows the similar CV curve except that the anodic peak at 0.35 V is inconspicuous. For the CV curve of Si/PVDF, the anodic peak at 0.35 V disappeared, which indicated that the lithiation and delithiation reactions were irreversible. For all of the electrodes, the peaks at 0.25 V which appeared at the third cycle were assigned to a crystal-to-amorphous transition.[43]

Fig. 4a shows the first discharge–charge profiles of Si electrodes using PVDF, PAA-PEO-PAA and PDA-PAA-PEO as binders at 0.01–1.0 V at a current density of 0.05 C. The discharge curve displayed a plateau profile at 0.1–0.01 V, consistent with the behavior of lithium-ion insertion.[44] The initial discharge capacities of Si/PDA-PAA-PEO and Si/PAA-PEO-PAA were 2983 and 3344 mA h g^{-1} with coulombic efficiencies (CEs) of 74% and 80% (Table 2), respectively; however, the Si/PVDF electrode delivered a discharge capacity of 2777 mA h g^{-1} with a CE of 68%. Moreover, the CEs of Si/PDA-PAA-PEO and Si/PAA-PEO-PAA electrodes increased to 98% at the fifth cycle, but the Si/PVDF electrode showed a CE of 92% at the fifth cycle (Fig. 4b). The higher CEs of Si/PDA-PAA-PEO and Si/PAA-PEO-PAA electrodes could be ascribed to the formation of a relatively stable SEI layer on the Si surface at the first lithium insertion/extraction.[45] Fig. 4c shows the cyclic charge–discharge

Table 1 Elemental analysis of PtBA-PEO-PtBA, PAA-PEO-PAA and PDA-PAA-PEO

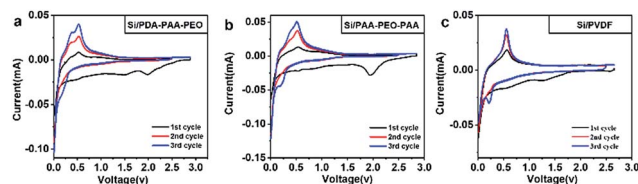|	N%	C%	H%	S%
PtBA-PEO-PtBA	0	64.76	10.373	0
PAA-PEO-PAA	0	47.48	6.874	0.284
PDA-AA-EO	1.31	40.76	6.08	0

Fig. 3 Cyclic voltammograms of Si electrodes made with PDA-PAA-PEO (a), PAA-PEO-PAA (b), PVDF (c) binders.

Fig. 4 Electrochemical properties of Si electrodes made with PDA-PAA-PEO, PAA-PEO-PAA and PVDF.

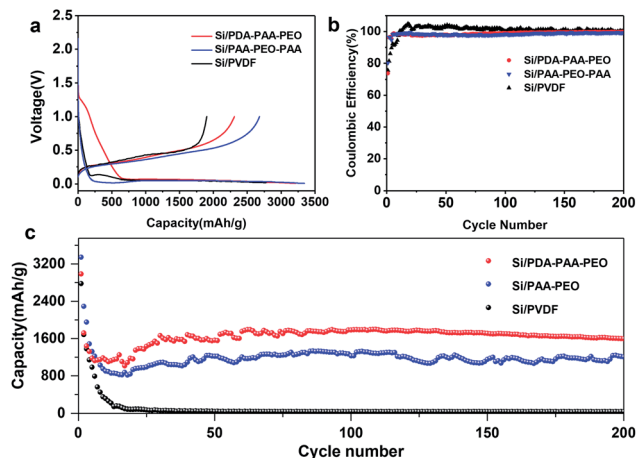Fig. 5 Nyquist plots of Si nanoparticle electrodes with PDA-PAA-PEO, PAA-PEO-PAA and PVDF.

curves of Si/PVDF, Si/PAA-PEO-PAA and Si/PDA-PAA-PEO at a current density of 0.5 C. The Si/PDA-PAA-PEO electrode exhibited quite a high capacity of 1597 mA h g^{-1} after 200 cycles, which was higher than that of the Si/PAA-PEO-PAA electrode with a capacity of 1205 mA h g^{-1} over 200 cycles, and the Si/PVDF electrode had a capacity of 40 mA h g^{-1} after 50 cycles. These results suggested that PDA-PAA-PEO could improve the electrochemical performance of the electrode effectively. The improvement of electrochemical performance could be attributed to the intensive adhesive cohesive force of PDA-PAA-PEO due to the strong interaction between functional groups (carboxyl and catechol) and hydroxyl groups on the SI surface.[46–48] Furthermore, the higher ion conductivity of PEO blocks was beneficial for decreasing the interfacial charge transfer impedance of electrodes, which resulted in the high capacity of Si/PDA-PAA-PEO.[49,50]

To investigate further the electrochemical characteristics of binders, EIS was done between 10 kHz and 10 MHz. Fig. 5 reveals the Nyquist plots of Si nanoparticle electrodes with the three binders after three discharge–charge cycles at a current density of 0.05 C. The diameters of the semicircles in high-frequency and medium-frequency ranges reflect the SEI resistance and interfacial charge transfer impedance, respectively. The slope in the low-frequency range represents the ionic diffusion resistance.[40,51] Notably, PVDF showed a relatively high SEI resistance (130 Ω) according to the fitted semicircles, and

PDA-PAA-PEO with the lowest resistance (50 Ω). These results substantiate the notion that PDA-PAA-PEO can decrease the interfacial charge transfer impedance of electrodes due to the higher ion conductivity of PEO blocks.[51] Moreover, studies have shown that binders have important roles in connecting whole complex electrodes and maintaining the integrity of conductive networks, all of which can decrease the interfacial charge transfer impedance of electrodes effectively.[52] The 180° peeling test suggested that PDA-PAA-PEO with a strong cohesion force (Fig. 6) could decrease the interfacial charge transfer impedance of electrodes further.

Fig. 6a shows the force–displacement curves of the electrodes with PDA-PAA-PEO and PAA-PEO-PAA. We did not need to conduct an adhesion test for PVDF considering its poor electrochemical behavior and reported weak bonding force.[52] The average force of PDA-PAA-PEO was 1.76 N, much higher than that for PAA-PEO-PAA (1.31 N). Moreover, it is clearly observed from Fig. 6b that many particles were detached from Si/PAA-PEO-PAA laminates. These results suggest that PDA-PAA-PEO binder could allow the cohesion of Si particles to the Cu

Table 2 Electrochemical data of Si/PVDF, Si/PAA-PEO-PAA and Si/PDA-PAA-PEO electrodes at a current density of 0.5 C

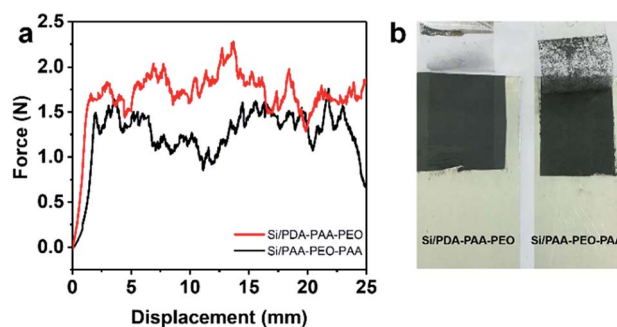|	Si/PVDF	Si/PAA-PEO-PAA	Si/PDA-PAA-PEO
Discharge capacity at 1st cycle (mA h g^{-1})	2777	3344	2983
Discharge capacity at 200th cycle (mA h g^{-1})	37	1205	1597
Initial coulombic efficiency (%)	68	80	74

Fig. 6 Peeling test of Si/PDA-PAA-PEO and Si/PAA-PEO-PAA laminates: (a) force–displacement curves. (b) Digital photograph of laminates after the peeling test.

current collector. The enhanced adhesive strength for PDA-PAA-PEO could be attributed to the strong interaction between functional groups (carboxyl and catechol) and hydroxyl groups on the Si surface. This is beneficial for decreasing the interfacial charge transfer impedance of electrodes and improves the electrochemical performance of the electrode. The results of the adhesion test were in agreement with that of the charge–discharge test (Fig. 4c). The Si/PDA-PAA-PEO electrodes exhibited ≈ 400 mA h g^{-1} larger capacities compared with that of Si/PDA-PAA-PEO, which was attributed to the enhanced adhesion by the catecholic interactions.

Conclusions

Triblock copolymer PDA-PAA-PEO containing the characteristics of ethylene oxide moieties as well as carboxyl and catechol groups was obtained *via* RAFT polymerization and a coupling reaction. The Si/PDA-PAA-PEO electrode exhibited excellent electrochemical performance with a quite high capacity of 1597 mA h g^{-1} after 200 cycles. The improvement of electrochemical performance could be attributed to the intensive adhesive cohesive force of PDA-PAA-PEO and higher ion conductivity of PEO blocks. Our research offers an environmentally friendly binder with excellent application prospects for the next generation of LIBs.

Conflicts of interest

There are no conflicts of interest to declare.

Acknowledgements

Notes and references

1 B. Scrosati, J. Hassoun and Y.-K. Sun, *Energy Environ. Sci.*, 2011, **4**, 3287.

2 H. Tao, L. Z. Fan, W. L. Song, M. Wu, X. He and X. Qu, *Nanoscale*, 2014, **6**, 3138–3142.

3 M.-S. Wang, W.-L. Song, J. Wang and L.-Z. Fan, *Carbon*, 2015, **82**, 337–345.

4 J. O. Besenhard, J. Yang and M. Winter, *J. Power Sources*, 1997, **68**, 87–90.

5 N. Liu, H. Wu, M. T. McDowell, Y. Yao, C. Wang and Y. Cui, *Nano Lett.*, 2012, **12**, 3315–3321.

6 S.-H. Ng, J. Wang, D. Wexler, K. Konstantinov, Z.-P. Guo and H.-K. Liu, *Angew. Chem., Int. Ed.*, 2006, **45**, 6896–6899.

7 M.-S. Wang, W.-L. Song and L.-Z. Fan, *J. Mater. Chem. A*, 2015, **3**, 12709–12717.

8 M.-S. Wang, W.-L. Song and L.-Z. Fan, *ChemElectroChem*, 2015, **2**, 1699–1706.

9 M.-S. Wang, Y. Song, W.-L. Song and L.-Z. Fan, *ChemElectroChem*, 2014, **1**, 2124–2130.

10 S. L. Chou, Y. Pan, J. Z. Wang, H. K. Liu and S. X. Dou, *Phys. Chem. Chem. Phys.*, 2014, **16**, 20347–20359.

11 G. Zhang, Y. Chen, Y. Deng, T. Ngai and C. Wang, *ACS Macro Lett.*, 2017, **6**, 641–646.

12 D. Mazouzi, Z. Karkar, C. Reale Hernandez, P. Jimenez Manero, D. Guyomard, L. Roué and B. Lestriez, *J. Power Sources*, 2015, **280**, 533–549.

13 M. A. Spreafico, P. Cojocaru, L. Magagnin, F. Triulzi and M. Apostolo, *Ind. Eng. Chem. Res.*, 2014, **53**, 9094–9100.

14 S. Komaba, K. Shimomura, N. Yabuuchi, T. Ozeki, H. Yui and K. Konno, *J. Phys. Chem. C*, 2011, **115**, 13487–13495.

15 A. Magasinski, B. Zdyrko, I. Kovalenko, B. Hertzberg, R. Burtovyy, C. F. Huebner, T. F. Fuller, I. Luzinov and G. Yushin, *ACS Appl. Mater. Interfaces*, 2010, **2**, 3004–3010.

16 S. Lim, H. Chu, K. Lee, T. Yim, Y. J. Kim, J. Mun and T. H. Kim, *ACS Appl. Mater. Interfaces*, 2015, **7**, 23545–23553.

17 J. Song, M. Zhou, R. Yi, T. Xu, M. L. Gordin, D. Tang, Z. Yu, M. Regula and D. Wang, *Adv. Funct. Mater.*, 2014, **24**, 5904–5910.

18 B. Koo, H. Kim, Y. Cho, K. T. Lee, N. S. Choi and J. Cho, *Angew. Chem., Int. Ed. Engl.*, 2012, **51**, 8762–8767.

19 Q. Lin, D. Gourdon, C. Sun, N. Holten-Andersen, T. H. Anderson, J. H. Waite and J. N. Israelachvili, *Proc. Natl. Acad. Sci. U. S. A.*, 2007, **104**, 3782–3786.

20 H. Lee, S. M. Dellatore, W. M. Miller and P. B. Messersmith, *Science*, 2007, **318**, 426–430.

21 S. Moulay, *Polym. Rev.*, 2014, **54**, 436–513.

22 Y. K. Jeong, S. H. Park and J. W. Choi, *ACS Appl. Mater. Interfaces*, 2017, DOI: 10.1021/acsami.7b08495.

23 L. Han, L. Yan, K. Wang, L. Fang, H. Zhang, Y. Tang, Y. Ding, L.-T. Weng, J. Xu, J. Weng, Y. Liu, F. Ren and X. Lu, *NPG Asia Mater.*, 2017, **9**, e372.

24 M. A. North, C. A. Del Grosso and J. J. Wilker, *ACS Appl. Mater. Interfaces*, 2017, **9**, 7866–7872.

25 M. H. Ryou, J. Kim, I. Lee, S. Kim, Y. K. Jeong, S. Hong, J. H. Ryu, T. S. Kim, J. K. Park, H. Lee and J. W. Choi, *Adv. Mater.*, 2013, **25**, 1571–1576.

26 F. Croce, G. B. Appetecchi, L. Persi and B. Scrosati, *Nature*, 1998, **394**, 456–458.

27 R. Kido, K. Ueno, K. Iwata, Y. Kitazawa, S. Imaizumi, T. Mandai, K. Dokko and M. Watanabe, *Electrochim. Acta*, 2015, **175**, 5–12.

28 C.-H. Tsao, C.-H. Hsu and P.-L. Kuo, *Electrochim. Acta*, 2016, **196**, 41–47.

29 T. Nakazawa, A. Ikoma, R. Kido, K. Ueno, K. Dokko and M. Watanabe, *J. Power Sources*, 2016, **307**, 746–752.

30 Y. H. Kwon, K. Minnici, M. M. Huie, K. J. Takeuchi, E. S. Takeuchi, A. C. Marschilok and E. Reichmanis, *Chem. Mater.*, 2016, **28**, 6689–6697.

31 M. Wu, X. Xiao, N. Vukmirovic, S. Xun, P. K. Das, X. Song, P. Olalde-Velasco, D. Wang, A. Z. Weber, L. W. Wang, V. S. Battaglia, W. Yang and G. Liu, *J. Am. Chem. Soc.*, 2013, **135**, 12048–12056.

32 S. J. Park, H. Zhao, G. Ai, C. Wang, X. Song, N. Yuca, V. S. Battaglia, W. Yang and G. Liu, *J. Am. Chem. Soc.*, 2015, **137**, 2565–2571.

33 N. Yuca, H. Zhao, X. Song, M. F. Dogdu, W. Yuan, Y. Fu, V. S. Battaglia, X. Xiao and G. Liu, *ACS Appl. Mater. Interfaces*, 2014, **6**, 17111–17118.

34 G. Zhang, Y. Chen, Y. Deng and C. Wang, *ACS Appl. Mater. Interfaces*, 2017, **9**, 36301–36310.

35 J. T. Lai, D. Filla and R. Shea, *Macromolecules*, 2002, **35**, 6754–6756.

36 Y. He and T. P. Lodge, *Macromolecules*, 2008, **41**, 167–174.

37 J. H. Ryu, J. W. Kim, Y.-E. Sung and S. M. Oh, *Electrochem. Solid-State Lett.*, 2004, **7**, A306–A309.

38 Y. Jin, S. Li, A. Kushima, X. Zheng, Y. Sun, J. Xie, J. Sun, W. Xue, G. Zhou, J. Wu, F. Shi, R. Zhang, Z. Zhu, K. So, Y. Cui and J. Li, *Energy Environ. Sci.*, 2017, **10**, 580–592.

39 B. Key, M. Morcrette, J.-M. Tarascon and C. P. Grey, *J. Am. Chem. Soc.*, 2010, **133**, 503–512.

40 N. Yuca and Ü. Çolak, *Electrochim. Acta*, 2016, **222**, 1538–1544.

41 J. Yoon, D. X. Oh, C. Jo, J. Lee and D. S. Hwang, *Phys. Chem. Chem. Phys.*, 2014, **16**, 25628–25635.

42 K. Liu, J. Zheng, G. Zhong and Y. Yang, *J. Mater. Chem.*, 2011, **21**, 4125.

43 M. Ge, J. Rong, X. Fang and C. Zhou, *Nano Lett.*, 2012, **12**, 2318–2323.

44 J. Liu, Q. Zhang, T. Zhang, J.-T. Li, L. Huang and S.-G. Sun, *Adv. Funct. Mater.*, 2015, **25**, 3599–3605.

45 S. P. V. Nadimpalli, V. A. Sethuraman, S. Dalavi, B. Lucht, M. J. Chon, V. B. Shenoy and P. R. Guduru, *J. Power Sources*, 2012, **215**, 145–151.

46 J. I. Lee, H. Kang, K. H. Park, M. Shin, D. Hong, H. J. Cho, N. R. Kang, J. Lee, S. M. Lee, J. Y. Kim, C. K. Kim, H. Park, N. S. Choi, S. Park and C. Yang, *Small*, 2016, **12**, 3119–3127.

47 H.-K. Park, B.-S. Kong and E.-S. Oh, *Electrochem. Commun.*, 2011, **13**, 1051–1053.

48 Y. Shi, X. Zhou and G. Yu, *Acc. Chem. Res.*, 2017, **50**, 2642–2652.

49 S. Lim, K. Lee, I. Shin, A. Tron, J. Mun, T. Yim and T.-H. Kim, *J. Power Sources*, 2017, **360**, 585–592.

50 M. Ling, J. Qiu, S. Li, C. Yan, M. J. Kiefel, G. Liu and S. Zhang, *Nano Lett.*, 2015, **15**, 4440–4447.

51 J. Guo, A. Sun, X. Chen, C. Wang and A. Manivannan, *Electrochim. Acta*, 2011, **56**, 3981–3987.

52 L. Zhang, L. Zhang, L. Chai, P. Xue, W. Hao and H. Zheng, *J. Mater. Chem. A*, 2014, **2**, 19036–19045.